CSIRO PUBLISHING

RESEARCH PAPER
https://doi.org/10.1071/WF25066

International Journal of WILDLAND FIRE
International Association of Wildland Fire

Offsetting the noise: a framework for applying phenological offset corrections in remotely sensed burn severity assessments

Casey E. Menick[A,*], Melanie K. Vanderhoof[A], Joshua J. Picotte[B], Alicia L. Reiner[C] and Robert A. Chastain[D]

For full list of author affiliations and declarations see end of paper

***Correspondence to:**
Casey E. Menick
U.S. Geological Survey, Geosciences and Environmental Change Science Center, Denver Federal Center, MS980, Denver, CO 80225, USA
Email: cmenick@usgs.gov

Received: 25 March 2025
Accepted: 18 November 2025
Published: 11 December 2025

Cite this: Menick CE *et al.* (2025) Offsetting the noise: a framework for applying phenological offset corrections in remotely sensed burn severity assessments. *International Journal of Wildland Fire* **34**, WF25066. doi:10.1071/WF25066

ABSTRACT

Background. Phenological correction of pre- and post-fire imagery is used to improve remotely sensed burn severity evaluations. Unburned offset values standardize greenness between image pairs; however, efficacy across diverse scenarios remains underexplored. **Aims.** We evaluated the impact of phenological offset correction methods to support analyst decision-making across fire-prone environments. **Methods.** We generated burn severity spectral index values for a dataset of Composite Burn Index (CBI) field plots across the conterminous US. The effectiveness of offset corrections was tested across image selection techniques, spectral indices, offset generation methods and burn perimeter sources. We assessed the influence of offset corrections on the modeled relationship with CBI, agreement between burn severity thresholds and potential bias. **Key results.** Applying offset corrections consistently improved the modeled relationship with CBI by addressing extreme outlier severity values. However, automated offset corrections had the potential to introduce bias, systematically lowering severity values and reducing correspondence with observed burn severity categories. **Conclusions.** Offset corrections offer benefits but also present trade-offs to accurately representing remotely sensed burn severity. **Implications.** The utility of offset corrections depends on the environment, methods and scale of analysis. We propose a decision-tree framework for analysts to consider when employing offset corrections given their study scope.

Keywords: burn severity, CBI, Composite Burn Index, Landsat, Normalized Burn Ratio, NBR, offset corrections, post-fire analysis, remote sensing, wildfire, wildland fire.

Introduction

Burn severity evaluations are crucial to characterize the ecological impacts of fire on wildlife habitat quality (Fontaine and Kennedy 2012; Lewis *et al.* 2022; Steel *et al.* 2022), hydrogeomorphology (Shakesby and Doerr 2006; Moody *et al.* 2008; Vieira *et al.* 2015; Rust *et al.* 2019; McGuire *et al.* 2024), carbon storage (Meigs *et al.* 2009; Yang *et al.* 2015; Hall *et al.* 2024) and vegetation condition (White *et al.* 1996; Lentile *et al.* 2007; Lydersen *et al.* 2016; Coop *et al.* 2020). Precise assessment of burn severity, the degree of fire impact on vegetation and soil organic matter (Keeley 2009), is necessary to support post-fire decision-making, including the prioritization of post-fire management efforts (Stevens-Rumann and Morgan 2019; Holden *et al.* 2022) and hazard mitigation (Staley *et al.* 2018; Dunn *et al.* 2019; Girona-García *et al.* 2021). Advances in satellite technology have enabled landscape-scale mapping of burned area (Giglio *et al.* 2018; Hawbaker *et al.* 2020) and severity (Eidenshink *et al.* 2007; Alonso-González and Fernández-García 2021), tracking trends in wildland fire through time (Dennison *et al.* 2014; Picotte *et al.* 2016) and associating field observations with satellite-derived characterizations of fire effects (Key and Benson 2006; Parks *et al.* 2019). Remotely sensed burn severity and vegetation change indices are increasingly crucial for monitoring wildland fire across the conterminous United States (CONUS), with the rising size and severity of wildfires in the western US (Parks and Abatzoglou 2020; Chandler *et al.* 2024), active application of prescribed fire in the southeastern US (Kobziar *et al.* 2015; Cummins *et al.* 2023) and greater

exposure to wildfire from an expanding wildland–urban interface (Wigtil *et al.* 2016; Radeloff *et al.* 2018; Hawbaker *et al.* 2023).

Burn severity is commonly evaluated using satellite-derived spectral indices based on the Normalized Burn Ratio (NBR), calculated from the shortwave-infrared (SWIR) and near-infrared (NIR) spectral wavelengths (García and Caselles 1991). NBR values are highly correlated with fire-induced vegetation change, where high SWIR reflectance from exposed soil (Lobell and Asner 2002) and low NIR reflectance from diminished healthy vegetation (Elvidge 1990) are indicative of greater fire effects. Burn severity change indices are calculated from the difference in spectral values measured before and after a fire, providing an estimation of the magnitude of the fire's impact. Commonly used metrics include the differenced NBR (dNBR; Key and Benson 2006), Relativized dNBR (RdNBR; Miller and Thode 2007), or Relativized Burn Ratio (RBR; Parks *et al.* 2014), where the latter two indices control for pre-fire vegetation abundance and condition. Pre- and post-fire imagery are typically derived from either manually selected image pairs (Key and Benson 2006) or mean composites of growing-season imagery (Parks *et al.* 2018*a*; Holsinger *et al.* 2022). Automated processing of satellite imagery has the capacity to rapidly quantify burn severity across wide spatial and temporal extents (Parks *et al.* 2018*a*; Picotte 2020; Alonso-González and Fernández-García 2021; He *et al.* 2024), enhancing our ability to characterize fire effects at national to global scales. In addition to generating burn severity from spectral indices alone, machine and deep learning approaches are being developed to more robustly model burn severity from multiple spectral bands and indices (Parks *et al.* 2019; Farasin *et al.* 2020; Partheepan *et al.* 2025; Vanderhoof *et al.* 2025). However, regardless of whether burn severity is evaluated by spectral indices or machine learning models, key decisions during image processing, such as imagery selection or choice of burn severity metric, can impact the reliability of burn severity measures (Cansler and McKenzie 2012; Holsinger *et al.* 2022; Howe *et al.* 2022) and the relationship with field observations of burn severity, such as the Composite Burn Index (CBI; Key and Benson 2006; Picotte *et al.* 2019).

Accounting for variation in vegetation condition between pre- and post-fire imagery is necessary to ensure that observed spectral changes accurately represent fire effects, rather than extraneous environmental variation. Image selection techniques seek to minimize differences in vegetation greenness by utilizing image pairs from closely matched time periods during the growing season (Key 2005; Parks *et al.* 2018*a*). Multivariate burn severity models may include unburned training points, additional image time points, or other environmental variables to similarly account for phenological variance (Meddens *et al.* 2016; Collins *et al.* 2018; Gibson *et al.* 2020; Vanderhoof *et al.* 2025). Despite efforts to standardize pre- and post-fire imagery, background spectral differences may persist owing to interannual variations in phenology, climate, disturbance, or image quality. For single-index measures of burn severity, an image offset value is often calculated to quantify the difference in vegetation condition between pre- and post-fire images (Key and Benson 2006; Miller and Thode 2007), computed as the spectral change (e.g. dNBR) of unburned areas outside the fire perimeter. Unburned areas may be identified manually (Key and Benson 2006; Collins *et al.* 2018; Picotte *et al.* 2020) or through automated approaches (Parks *et al.* 2018*a*; Picotte 2020). Image offset values were introduced to assess the suitability of pre- and post-fire image pairs, with images ideally exhibiting a dNBR of zero in unburned areas. Incorporating the unburned offset value into the calculation of dNBR has been shown to improve the relationship with CBI and make more analogous comparisons across fires (Miller and Thode 2007; Miller *et al.* 2009; Parks *et al.* 2014; Reiner *et al.* 2022); however, benefits are not consistently identified across studies (Picotte and Robertson 2011; Howe *et al.* 2022; Morresi *et al.* 2022; Vanderhoof *et al.* 2025).

Further research on the impact of offset corrections in remotely sensed burn severity evaluations is necessary to characterize their efficacy and generalizability. The utilization of offset values in burn severity calculations remains inconsistent, with approximately half of analyses applying corrections (Miller *et al.* 2023). Furthermore, the application of an image offset value has been theorized to introduce additional error depending on a variety of factors. The applicability of automated offset corrections has been specifically cautioned in landscapes with diverse cover types (Parks *et al.* 2018*a*), adjacent disturbances (Whitman *et al.* 2020), or unclear burn perimeters (Parks *et al.* 2019), although concerns have not been empirically tested. Very few studies explicitly consider the benefit or limitations of applying image offset corrections in burn severity calculations (Miller *et al.* 2023).

Our study provides a comprehensive evaluation of the influence of offset corrections in remotely sensed burn severity calculations, addressing key data gaps and proposing a decision-tree framework to support remote sensing analysts. We evaluate the efficacy of offset corrections across the most commonly utilized manual and automated approaches to measure burn severity, comparing across choice of burned area dataset, offset generation method, image selection process and spectral indices utilized. Understanding how methodological choices interact and compound uncertainty across diverse, fire-prone ecosystems is essential to ensure reliability and generalizability of burn severity assessments (Stambaugh *et al.* 2015; Miller *et al.* 2023). We evaluated the relationship between Landsat satellite-derived burn severity measures and a dataset of CBI field plots (Picotte *et al.* 2019) to characterize the impact of image offset corrections for a wide range of fire-prone ecosystems across CONUS. Our research questions included:

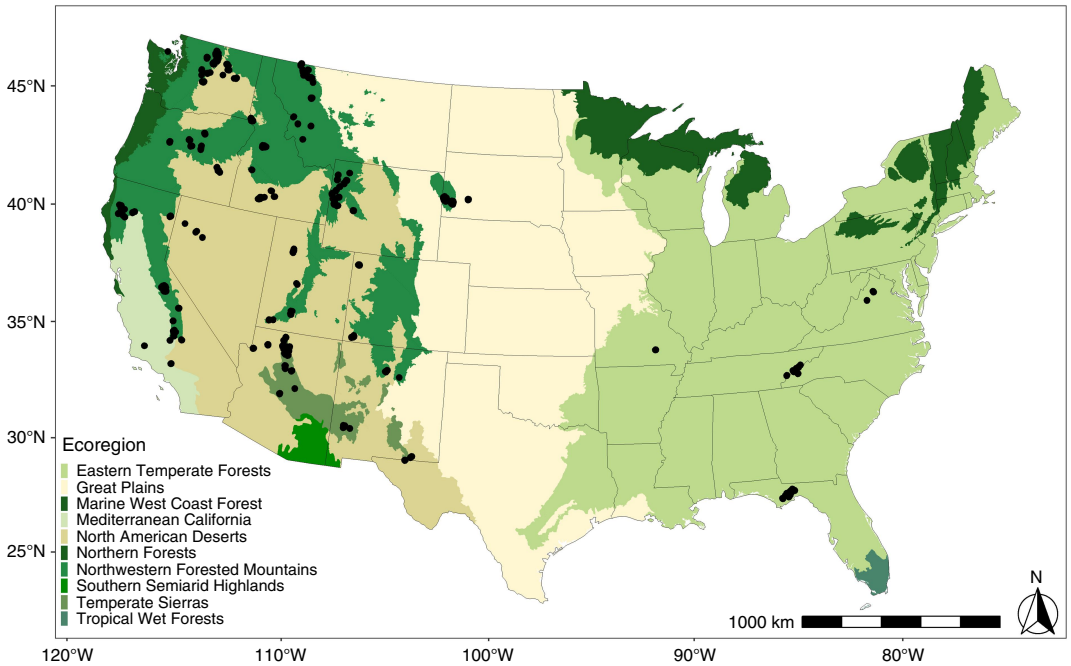

Fig. 1. Distribution of Composite Burn Index (CBI) field plots by ecoregions of the conterminous United States that are mapped by both the Landsat Burned Area Product (LBA) and Monitoring Trends in Burn Severity (MTBS) datasets.

1. How do image offset corrections impact the modeled relationship between field-observed and remotely sensed measures of burn severity?
2. How do the stability, bias and accuracy of offset corrections vary across methodological choices?
3. How do landcover characteristics influence the usefulness of offset corrections?

Materials and methods

Study area and field data

We evaluated the relationship between remotely sensed and field-observed burn severity using a compiled collection of CBI field plots (Fig. 1; Picotte *et al.* 2019). CBI is commonly used to evaluate fire severity across soil and vegetation strata on a continuous range from 0, signifying unburned conditions, up to 3, representing complete biomass consumption (Key and Benson 2006). Field plots were assembled from an array of collection efforts (1994–2017) following 234 fire events across CONUS. CBI plots were predominantly collected following wildfires in the western US; however, plots do encompass a wide range of fire-prone landscapes, providing a robust data source to support burn severity modeling (Miller *et al.* 2023). The dataset captures the full range of CBI burn severity values (0–3), with a mean CBI of 1.47 and a standard deviation of 0.88.

Across the evaluated CBI plots, annual precipitation averaged 703 mm (range of 187–1751 mm), with average minimum and maximum temperatures of 1.5 and 15.7°C (1990–2020; Abatzoglou *et al.* 2018). Landcover, as defined by the National Land Cover Database (NLCD; US Geological Survey 2025), was predominantly evergreen forest (75.4%), shrub–scrub (13.8%), grassland–herbaceous (4.6%) and woody wetlands (2.8%). Dominant forest groups (Ruefenacht *et al.* 2008) represented by the CBI data included ponderosa pine (25.3%), Douglas-fir (15.6%), fir–spruce–mountain hemlock (13.8%), pinyon–juniper (9.2%), lodgepole pine (10.0%), longleaf–slash pine (8.1%) and California mixed conifer (5.8%).

Burned area datasets

We obtained burned area perimeters from (1) Monitoring Trends in Burn Severity (MTBS; 30 m spatial resolution; Eidenshink *et al.* 2007) and (2) the Landsat Burned Area product (LBA; 30 m spatial resolution; Hawbaker *et al.* 2020), the two moderate-resolution products with full coverage across CONUS. The MTBS program maps all wildland fires greater than 400 ha in the western US and 200 ha in the eastern US, with fire perimeters manually digitized by analysts using dNBR or NBR imagery (Key and Benson 2006; Eidenshink *et al.* 2007). The LBA product uses a burn-detection algorithm to map wildfires and prescribed fires >2 ha across CONUS, with omission and commission errors of 19 and 41%, respectively (Hawbaker *et al.* 2020). We included comparison with LBA to represent an automated burned area product, as these are increasingly relied on, relative to perimeter datasets, and provide more complete

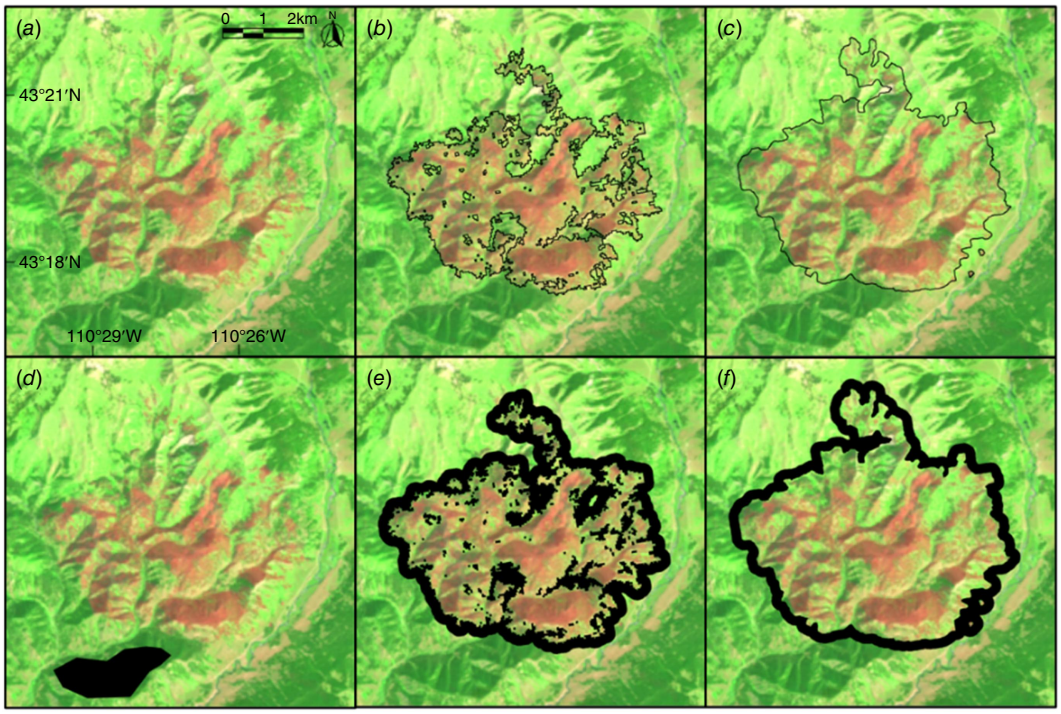

Fig. 2. Example of an identified fire event (*a*), and corresponding burned (*b, c*), and unburned (*d–f*) areas used in the calculation of burn severity. (*a*) Landsat 5 post-fire mean image composite collected June–September 2001, displayed with a false color composite using shortwave infrared 2, near-infrared and red bands to highlight fire effects. Burned area polygons for the fire, delineated by (*b*) the Landsat Burned Area (LBA) product, and (*c*) Monitoring Trends in Burn Severity (MTBS) datasets. Examples of unburned areas, commonly used to calculate burn severity offset values, are shown in black and include (*d*) a manually delineated unburned polygon of similar vegetation composition to the fire event, as well as an automated ring buffer (180 m outer, 0 m inner) surrounding (*e*) LBA, and (*f*) MTBS fire perimeters.

mapping of small and prescribed fires, with greater spatial and temporal consistency (Chuvieco *et al.* 2019). Pixels identified as burned by the algorithm were consolidated into burned area polygons on an annual basis. Consequently, LBA perimeters for a single fire event may comprise many small, discontiguous burned areas (Fig. 2*b*), whereas MTBS perimeters are more typically one single polygon with inclusions of unburned areas (Fig. 2*c*; Kolden and Weisberg 2007; Meddens *et al.* 2016). Both datasets provide temporal information as either a recorded ignition date (MTBS) or the first burn detection date (LBA).

We identified MTBS perimeters corresponding to CBI field plot records from spatially matching records within the same burn year. We obtained LBA perimeters using a similar process, additionally including discontiguous burn polygons if located either within 1 km or the footprint of a corresponding MTBS perimeter and having burn dates within 1 month. In a few cases where fire events denoted by the CBI dataset were mapped as a single event by LBA, burned area polygons were consolidated. Out of the 234 fires within the CBI dataset, we were able to identify 171 fire perimeters from MTBS and 183 from LBA that had had spatially matching records at the CBI plot locations. We conducted our evaluation across the 141 fire events recorded by both products (Fig. 1), specifically on the shared set of CBI plots (n = 4369) that fell within both MTBS and LBA perimeters to make equivalent comparisons between datasets. Matched CBI data included unburned control plots (n = 292) if points were located within both fire polygons.

Unburned offset areas

For each of the 141 fire events, we identified corresponding unburned areas to calculate image offset values. Unburned areas are ideally located near the fire perimeter with similar vegetation composition to best represent phenological differences between pre- and post-fire image timepoints. We generated offset values using both manual (Key and Benson 2006) and automated (Parks *et al.* 2018*a*) methods to compare two commonly utilized approaches.

Manual identification of unburned areas involves visually inspecting imagery to identify comparable vegetation unaffected by fire outside the fire perimeter (Key and Benson 2006). For our analysis, we utilized the analyst-generated unburned offsets provided within the MTBS

Table 1. Satellite spectral indices and offsets used to calculate burn severity and compare performance across methodologies.

	Calculation	Formula	Reference
(a)	Normalized Burn Ratio (NBR)	$NBR = \frac{NIR - SWIR}{NIR + SWIR}$	García and Caselles (1991)
(b)	differenced NBR (dNBR)	$dNBR = (NBR_{prefire} - NBR_{postfire}) \times 1000$	Key and Benson (2006)
(c)	Relativized dNBR (RdNBR)	$RdNBR = \begin{cases} \frac{dNBR}{\sqrt{\lvert NBR_{prefire}\rvert}}, & \lvert NBR_{prefire}\rvert \geq 0.001 \\ \frac{dNBR}{\sqrt{\lvert 0.001\rvert}}, & \lvert NBR_{prefire}\rvert < 0.001 \end{cases}$	Miller and Thode (2007)
(d)	dNBR Offset ($dNBR_{offset}$)	$dNBR_{offset} = dNBR - dNBR_{unburned}$	Key and Benson (2006)
(e)	RdNBR Offset ($RdNBR_{offset}$)	$RdNBR = \begin{cases} \frac{dNBR_{offset}}{\sqrt{\lvert NBR_{prefire}\rvert}}, & \lvert NBR_{prefire}\rvert \geq 0.001 \\ \frac{dNBR_{offset}}{\sqrt{\lvert 0.001\rvert}}, & \lvert NBR_{prefire}\rvert < 0.001 \end{cases}$	Miller and Thode (2007)

thematic severity product metadata for each fire (Eidenshink *et al.* 2007). MTBS analysts derive offsets from polygons composed of hundreds to thousands of pixels representative of the vegetation within the fire extent, considering the stratification of vegetation composition (Fig. 2*d*; Eidenshink *et al.* 2007).

Automated approaches typically use a buffered ring around fire perimeters to identify nearby unburned vegetation, presumed to be similar in composition (Fig. 2*e–f*; Parks *et al.* 2018*a*; Whitman *et al.* 2020; Howe *et al.* 2022; Saberi and Harvey 2023). Following Parks *et al.* (2018*a*), we generated ring buffers surrounding all MTBS and LBA fire perimeters using a range of distances. Outer buffer distances, the maximum distance from the fire perimeter, included 100, 180, 250, 500 and 1 km. Although 180 m is a commonly used outer buffer size with MTBS fire perimeters (Fig. 2*e–f*; Parks *et al.* 2018*a*), we wanted to consider differences from the LBA product, which has not previously been examined. We also tested the use of inner buffer distances, a set minimum distance from the fire perimeter (0, 50, 100 and 250 m), to examine potential edge effects, for a total of 17 different buffer sizes.

Burn severity calculation

Remotely sensed burn severity was evaluated using Landsat 5–8 TM, ETM+ (Enhanced Thematic Mapper) and OLI (Operational Land Imager) imagery obtained from Google Earth Engine. We generated pre- and post-fire NBR images from (1) manually selected scene pairs used by the MTBS program for burn severity evaluation (Eidenshink *et al.* 2007) and (2) an automated annual mean image compositing approach (Parks *et al.* 2018*a*). These two image selection methods represent the two most common approaches used by remote sensing analysts to assess burn severity. Scene pair selection allows greater analyst control to select the best-matched, error-free and representative images of pre- and post-fire conditions. Compositing imagery eliminates the need for manual scene selection and may be more robust to variations in vegetation greenness and outlier spectral values by incorporating observations from multiple time points. Manually selected scene pairs were identified from the corresponding MTBS metadata for each recorded fire. The automated method generated pre- and post-fire composite images following Parks *et al.* (2018*a*) in Google Earth Engine, a widely utilized and easily deployable burn severity processing framework. Following these methods, composite images were derived from pixel-wise mean growing-season NBR values for the years before and after the fire event. The growing season was defined as April–June in Arizona, New Mexico, Utah and Nevada, and June–September for all other states to best align with peak vegetation greenness and expected fire seasonality, snow cover and cloud cover identified by Parks *et al.* (2018*a*).

CFMask was used from the scene-reported pixel quality assurance (QA) bands to exclude cloud, cloud shadow, water and snow from all Landsat imagery used (Foga *et al.* 2017). We considered the full range of pixel values, with no further image masking, to remain consistent with established methods. Spectral indices representing burn severity, dNBR and RdNBR were derived for all CBI plots from overlapping pixel values using the two image selection approaches (Table 1). Although numerous spectral indices have been used to quantify burn severity, dNBR and RdNBR are the two most commonly employed (Miller *et al.* 2023), are operationally distributed by the MTBS program (Eidenshink *et al.* 2007), are the foundation available global burn severity datasets (Alonso-González and Fernández-García 2021; He *et al.* 2024) and provide opportunity to examine differences between absolute and relativized burn severity measures (Miller and Thode 2007). Furthermore, these indices commonly show strong variable importance within machine learning modeling approaches (e.g. Gibson *et al.* 2020; Vanderhoof *et al.* 2025). Corresponding unburned offset values were also calculated for each fire from the mean dNBR pixel value within each identified ring buffer area. We subsequently derived $dNBR_{offset}$ and $RdNBR_{offset}$ indices for all CBI plots by subtracting the corresponding automatically derived

or MTBS-provided $dNBR_{unburned}$ values from dNBR (Table 1). As MTBS reports the offset value without a reference polygon, we conducted our evaluation of manually delineated offsets using only the scene pair selection method.

Regression model performance

We used non-linear least squares (NLS) exponential regression to model the continuous relationship between CBI and spectral indices, including dNBR, RdNBR and their offset-adjusted variants $dNBR_{offset}$ and $RdNBR_{offset}$ (Eqn 1; Miller and Thode 2007):

$$y = a + b \times \exp(\text{CBI} \times c) \quad (1)$$

Model parameters (a, b, c) were derived separately for each spectral index (y). Although many model types have been used to characterize the association between field and satellite measures of severity (Miller *et al.* 2023), the exponential regression form describes the relationship with balanced performance across the full range of severity values. Similar spectral indices (e.g. dNBR, RdNBR) are relied on for the generation of burn severity, whether from a single spectral index or a machine learning or deep learning algorithm. However, algorithms can also be influenced by model complexity and parameterization, making it difficult to isolate the impact of individual methodological choices. Therefore, we used a more simplistic regression approach to support broader applicability across modeling methods and study scopes. We evaluated the performance of each spectral index using the corresponding model root mean square error (RMSE), across (1) paired scene selection and mean annual image compositing approaches, (2) automated and manual unburned offset area delineation, (3) MTBS and LBA fire perimeter sources, and (4) dNBR and RdNBR spectral indices.

Offset correction influence on stability, bias and accuracy

To assess the stability, bias and accuracy of offset corrections, we evaluated the impact of offset correction using the two most commonly used offset generation methods, manual delineation (Fig. 2*d*; Key and Benson 2006) and an automated ring buffer method, using 180 m outer and 0 m inner distances (Fig. 2*e–f*; Parks *et al.* 2018*a*). We evaluated the stability of offset corrections by comparing the distribution of residual values between models generated using (1) dNBR and $dNBR_{offset}$, and (2) RdNBR and $RdNBR_{offset}$. For each, we calculated the difference in mean and standard deviation of absolute error values, along with the proportion of CBI plots showing improved error metrics following offset correction. All significant differences were assessed using the Mann–Whitney U test. More stable offset corrections would exhibit lower variability, consistent improvements in mean squared error, and higher proportions of plots with decreased residuals.

To investigate any sources of systematic bias, we evaluated the distribution of $dNBR_{unburned}$ offset values generated for all 141 fire events. Compared across many fire events, $dNBR_{unburned}$ values should average to zero and generally fall between -50 and 50 if representative of unchanged, background vegetation conditions (Key and Benson 2006; Picotte 2020). We conducted one-sample t-tests to identify any directional bias in $dNBR_{unburned}$, testing if mean $dNBR_{unburned}$ values across all 141 fire events significantly differed from zero. Offset correction methods that introduce bias into the characterization of burn severity would be expected to exhibit a directional shift on burn severity valuation.

Finally, we compared classification accuracy between spectral indices produced with and without offset corrections. CBI values were defined as Unburned (CBI = 0), Low ($0 < \text{CBI} < 1.25$), Moderate ($1.25 \leq \text{CBI} < 2.25$) and High ($\text{CBI} \geq 2.25$) following Key and Benson (2006). Spectral index thresholds were determined individually from CBI class values using each index's respective NLS regression. For dNBR and $dNBR_{offset}$, we also compared classification accuracy using the fire-specific severity thresholds set by MTBS analysts to make standard comparisons across fires. We assessed significant differences in classification accuracy across all fire events using paired t-tests.

Offset performance across environmental scenarios

To assess where offset corrections had the largest influence on model performance, we evaluated differences in model RMSE across environmental characteristics using the annual NLCD landcover and total canopy cover datasets (US Geological Survey 2025). All data were obtained from the respective pre-fire year to best represent vegetation conditions. We compared model performance across dominant landcover categories, including evergreen forest, grassland, shrub–scrub and woody wetlands, but were unable to assess performance for less-represented types in the dataset, such as mixed and deciduous forests. Canopy cover was compared for classes of closed canopy (≥70% cover), open canopy (10–70% cover) and non-forested (≤10% cover). We evaluated the overall impact of offset correction on model performance for each of these classes, as well as the influence of heterogeneity and non-representative cover types within the derived offset area. Heterogeneity was defined from the standard deviation of canopy cover and the Shannon index of NLCD classes within each offset area. Representativeness was defined as the proportion of the canopy cover or landcover within the offset area matching each respective CBI plot. We defined high or low strata of heterogeneity and representativeness from the median values across the 141 fire events. We calculated RMSE between

high and low heterogeneity and representativeness classes to compare differences in model error.

Results

Comparison of regression model performance

Offset correction of dNBR led to consistent improvements in the modeled relationship between remotely sensed spectral indices and field-observed burn severity (Fig. 3). For all tested offset generation methods and methodological decision-points, $dNBR_{offset}$ (mean RMSE 156.6) and $RdNBR_{offset}$ (mean RMSE 447.4) resulted in significantly lower RMSE values relative to uncorrected dNBR (mean RMSE 165.6) and RdNBR (mean RMSE 464.0). Among automatically derived offsets, applying corrections derived from LBA ring buffers typically resulted in lower model errors relative to those derived from MTBS perimeters (Fig. 3). Offset buffer distances also impacted performance, with consistently lower RMSE values observed from offsets derived using smaller inner and outer buffer distances. The overall best-performing ring buffer offset (RMSE 142.8) utilized a 100 m outer and 0 m inner buffer (Fig. 4), followed closely by the commonly used 180 m outer and 0 m inner buffer (RMSE 143.5; Fig. 3). Offset corrections had larger benefits when using composite imagery relative to the paired scenes and when using RdNBR relative to dNBR. The manually delineated offset produced RMSE values comparable with the automatically derived buffer offsets, indicating similar efficacy of the two approaches. Overall, other methodological choices, such as image selection method or spectral index, had a larger impact on model performance than offset correction. In particular, RdNBR-based models had two to three times larger RMSE values than dNBR-based models, exceeding the relative difference in magnitude between the indices.

Stability of offset corrections

The stability of offset corrections, as measured by the variability in model residual values, showed that manually delineated offsets provided the most consistent improvements (Fig. 5). In contrast, the 180 m buffer offsets showed higher variability, particularly for those derived from LBA perimeters. Offset correction of RdNBR also resulted in significantly greater residual variability, whereas residual values between dNBR and $dNBR_{offset}$ models were comparatively more consistent. Across all methodological decision-points, the improvements in model error from offset corrections were primarily driven by poorly predicted plots with high residual values (Fig. 5). Applying offset corrections to dNBR reduced residual values for a narrow majority of plots across methods (50.1–59.0%), indicating the correction also led to poorer prediction for a substantial subset of plots (Fig. 5).

Potential of bias within offset corrections

To evaluate potential systematic bias introduced by offset corrections, we examined the distribution of $dNBR_{unburned}$ values across all 141 fire events. The automatically derived buffer offset values exhibited a positive bias, influenced by buffer distance (Figs 6, 7). One-sample *t*-tests showed that mean $dNBR_{unburned}$ values were significantly greater than zero (+7.3–86.6) for all buffer distances and calculation methods tested. The positive bias was reduced by using larger inner and outer buffer sizes or when evaluating a greater number of pixels further from the fire edge (Fig. 6). We observed greater positive biases in $dNBR_{unburned}$ values derived from LBA perimeters, relative to MTBS perimeters ($\Delta dNBR_{unburned}$ = 31.8), and when using paired scene selection, relative to using image compositing ($\Delta dNBR_{unburned}$ = 5.05; Figs 6, 7). Mean and median offset values were highly similar across all tested comparisons. Conversely, manually delineated offsets did not exhibit any bias, with mean $dNBR_{unburned}$ offset values insignificantly different from zero, suggesting adequate representation of undisturbed vegetation (Fig. 7).

Offset correction influence on severity classification accuracy

Utilizing model-specific regression thresholds, overall burn severity classification accuracy by dNBR and RdNBR was largely similar with or without offset correction, with accuracy ranging from 53.4 to 56.1% (Table 2). Offset correction offered modest improvements in overall classification accuracy for most comparisons; however, these differences were largely statistically insignificant compared across fire events. Impacts of offset correction did not have a consistent impact across levels of burn severity, although classification of unburned and low-severity classes saw both the largest positive and negative impacts of offset correction.

Applying the fire-specific dNBR thresholds provided by MTBS yielded more substantial differences in classification accuracy following offset correction (Table 2). When compared with a standard set of burn severity thresholds, automated buffer offset corrections exhibited a significant negative influence on overall classification accuracy. Shifts in severity classification were predominantly (77.8–97.8%) to lower-severity classes, following the bias observed in the $dNBR_{unburned}$ values. Negative impacts were disproportionately observed within lower-severity classes and image composites, where unburned classification saw a significant improvement. Conversely, dNBR correction by the manually delineated offset values did not exhibit significant differences in classification accuracy

Offset influence across environmental scenarios

Finally, we examined the influence of offset corrections on model performance across vegetation conditions. Overall, offset corrections reduced model RMSE for almost all

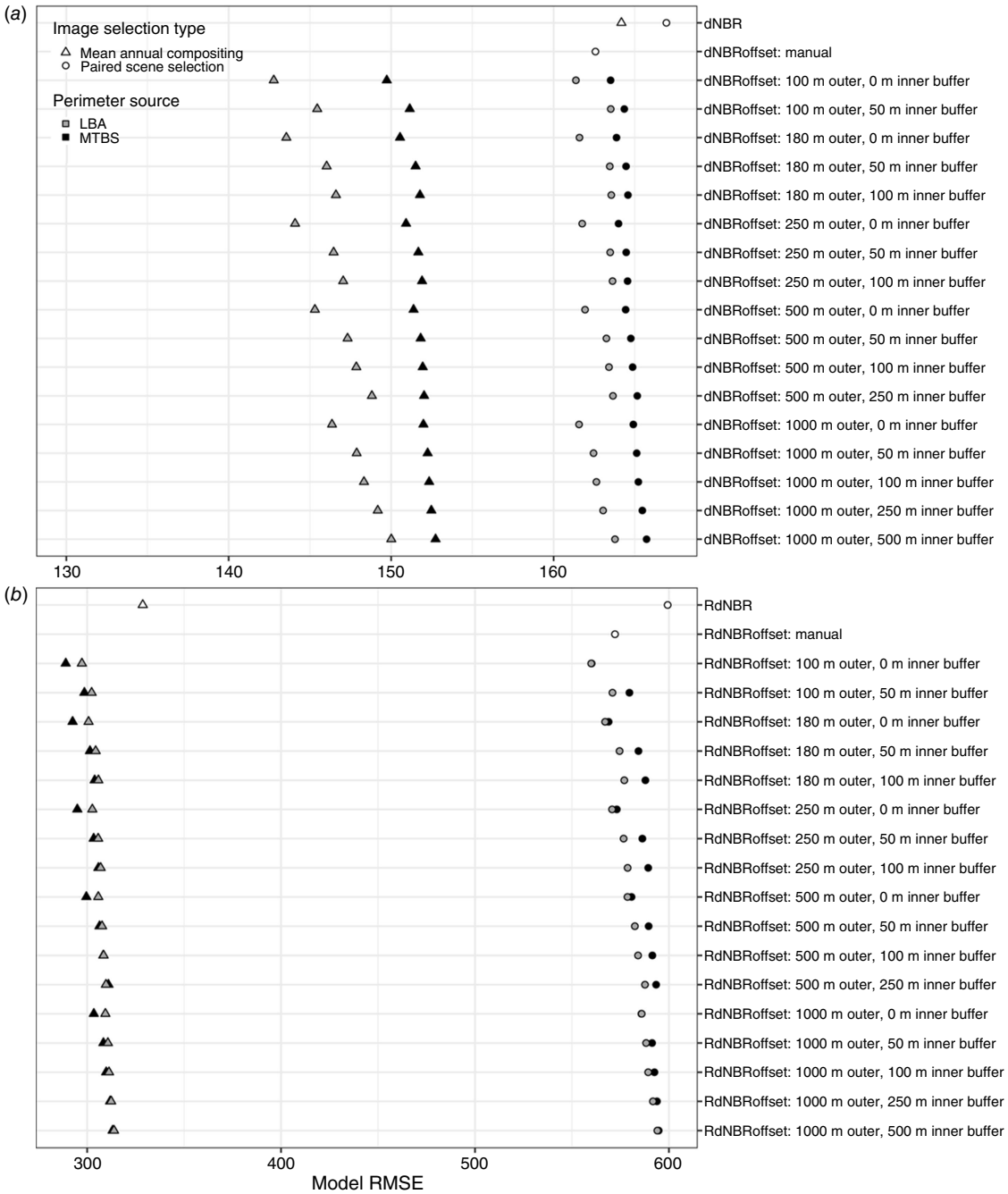

Fig. 3. Performance of models relating field-collected Composite Burn Index (CBI) and satellite-derived burn severity measures. We contrast model RMSE from (*a*) dNBR (differenced Normalized Burn Ratio), and (*b*) RdNBR (Relativized dNBR) values with and without offset correction across spectral indices, image selection method and offset type used. Offsets generated manually (white) and from ring buffers surrounding Monitoring Trends in Burn Severity (MTBS; black) and Landsat Burned Area (LBA; gray) fire perimeter datasets are evaluated.

canopy and landcover classes, improving model performance (Tables 3, 4). The only significant increase in model RMSE following offset corrections occurred from CBI plots within woody wetlands when evaluated using paired scene imagery. The largest consistent landcover-specific reductions in RMSE were observed within shrub–scrub and grasslands (Table 3) and within non-forested canopy structures (Table 4). Patterns of RMSE across landcover and canopy cover classes were largely similar between dNBR and RdNBR, albeit at different magnitudes.

Vegetation composition within the offset area resulted in larger differences between spectral indices. While using

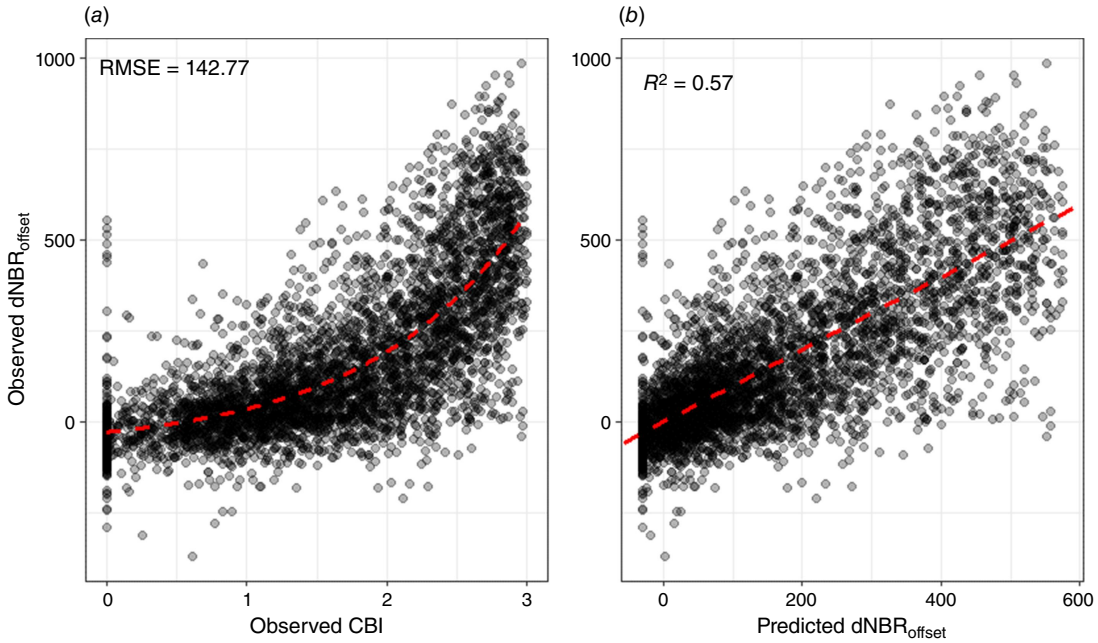

Fig. 4. The relationship between field-collected and satellite-derived burn severity data for the best-performing automatically generated buffer offset correction methodology. (*a*) Observed Composite Burn Index (CBI) burn severity and associated differenced Normalized Burn Ratio (dNBR) values calculated from mean annual image composites, offset with the unburned dNBR from a 100 m buffered ring surrounding Landsat Burned Area (LBA) fire perimeters. The red dashed line indicates the fitted exponential relationship between CBI and $dNBR_{offset}$, with associated root mean squared error (RMSE) shown. (*b*) Exponential model-predicted dNBR compared with associated observed $dNBR_{offset}$ values, with red dashed 1:1 identity line and associated R^2 value overlaid.

dNBR, buffer offset areas composed of more representative and homogeneous vegetation composition saw greater improvements from offset corrections, consistent across landcover and canopy cover classes (Tables 3, 4). The only contradictory findings were greater benefits observed in areas with unrepresentative vegetation for woody wetlands and heterogeneous canopy cover used to represent closed canopy forests. Using RdNBR, patterns were less consistent, with the majority vegetation classes conversely showing model improvement when offset areas included less representative or more heterogeneous vegetation (Tables 3, 4).

Discussion

Patterns of burn severity model performance

Across all comparisons of offset source, image selection and spectral indices evaluated, applying offset corrections dependably enhanced the overall modeled relationship between field-observed and remotely sensed burn severity measures. Our findings align with previous research (Miller and Thode 2007; Parks *et al.* 2014, 2018*a*) that applying dNBR offset corrections derived from 180 m ring buffers and manually delineated polygons are among the most effective methods to reduce model error. Although the influence of offset corrections on model performance was consistent, larger benefits were observed in specific methodological scenarios, such as when using image composites compared with paired scenes, or when using RdNBR relative to dNBR. Overall, however, the impact of offset corrections contributed less to model performance than other methodological decision-points, such spectral index or image selection strategy.

Although offset corrections improved overall model error, some resulted in less consistent outcomes. The notably larger variability observed in RdNBR-based models and from automatically generated offsets likely reflects a greater sensitivity to spectral irregularities. RdNBR may introduce additional uncertainty, as extreme values can arise from near-zero pre-fire NBR conditions, which may also explain the substantially poorer model performance relative to dNBR-based models. Automatically derived offsets, particularly those derived from LBA-perimeters, may also incorporate more spectral variability across the landscape. Greater uncertainty selecting purely undisturbed pixels representative of vegetation conditions is inherent to any automatically derived method or burned area product. The observed variability across methodological choices may in part explain the negative influence of offset corrections identified within

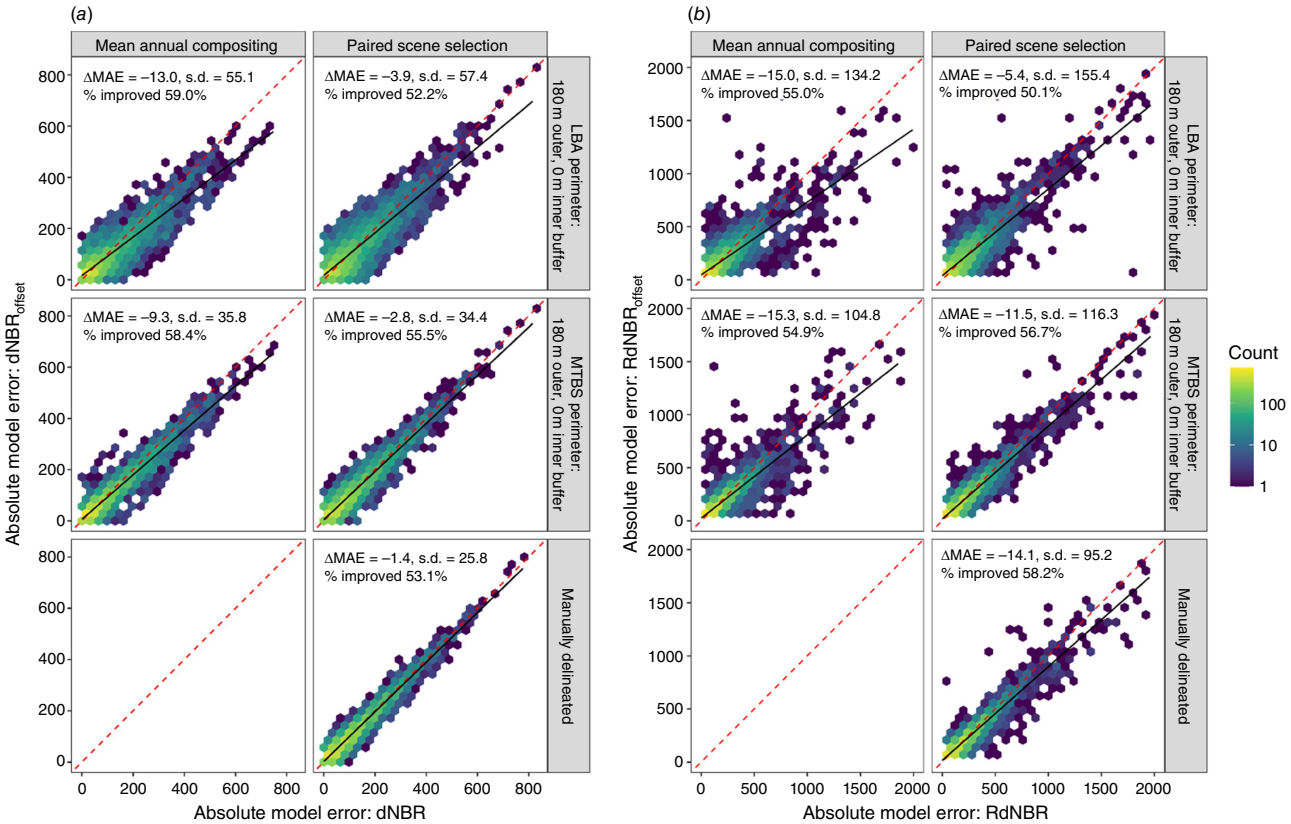

Fig. 5. Comparison of absolute model error values between (*a*) dNBR (differenced Normalized Burn Ratio) and (*b*) RdNBR (Relativized dNBR) and corresponding dNBR$_{offset}$ and RdNBR$_{offset}$ models. The dashed red line represents the 1:1 identity line; the solid black line represents the linear regression line. Points below the identity line indicate enhanced model performance when incorporating the offset value, whereas points above suggest a stronger relationship without an offset correction. The proportion of plots with improved model residuals, change in mean absolute error (ΔMAE) and s.d. of the difference in error values following offset correction are shown. Comparisons are included for manually delineated and ring buffer (180 m outer, 0 m inner) offsets surrounding Landsat Burned Area (LBA) and Monitoring Trends in Burn Severity (MTBS) burn perimeters for paired scene and composite image selection approaches. The range of values for RdNBR has been limited to improve data visibility, which excludes some extreme values.

some, relatively smaller-scale studies (Picotte and Robertson 2011; Howe *et al.* 2022; Morresi *et al.* 2022). Furthermore, we found model improvements following offset corrections were primarily driven by addressing high-error outlier values, rather than uniform improvement across the dataset, somewhat differing from the perspective that offsets provide consistent standardization of thresholds between fires (Miller and Thode 2007; Parks *et al.* 2014).

The influence of large offset corrections was also evident in model performance across environmental conditions, with greater improvements observed within ecosystems with larger variations in vegetation greenness. Although limited CBI plots prevented comparison within deciduous forests, non-forested ecosystems such as grasslands and shrub–scrub, also characterized by greater seasonal and interannual differences (Reed *et al.* 1994; Melaas *et al.* 2013), exhibited larger benefits and a greater magnitude of offset correction. In contrast, more densely canopied ecosystems and evergreen cover have more temporally consistent vegetation greenness (Wong and Gamon 2015; Ulsig *et al.* 2017), resulting in less beneficial offset corrections. The disparate impact of offset corrections within woody wetlands may stem from the influence of seasonal flooding or dynamic fire history (Picotte and Robertson 2011; Vanderhoof *et al.* 2021), which may interfere with single-scene imagery but be mitigated by image compositing techniques. Overall, image compositing was shown to provide more consistent outcomes and improved model performance by capturing greater variability, particularly within non-forested landcover types. dNBR-based models showed greater improvement when offsets were derived from homogeneous and representative vegetation, providing more consistent spectral values. In contrast, the pre-fire relativization of RdNBR likely mitigates that variability, resulting in improved model performance when more diverse landcover and canopy cover were considered. Ultimately, our findings suggest that spatial and temporal variability of vegetation greenness is an important consideration when characterizing burn severity,

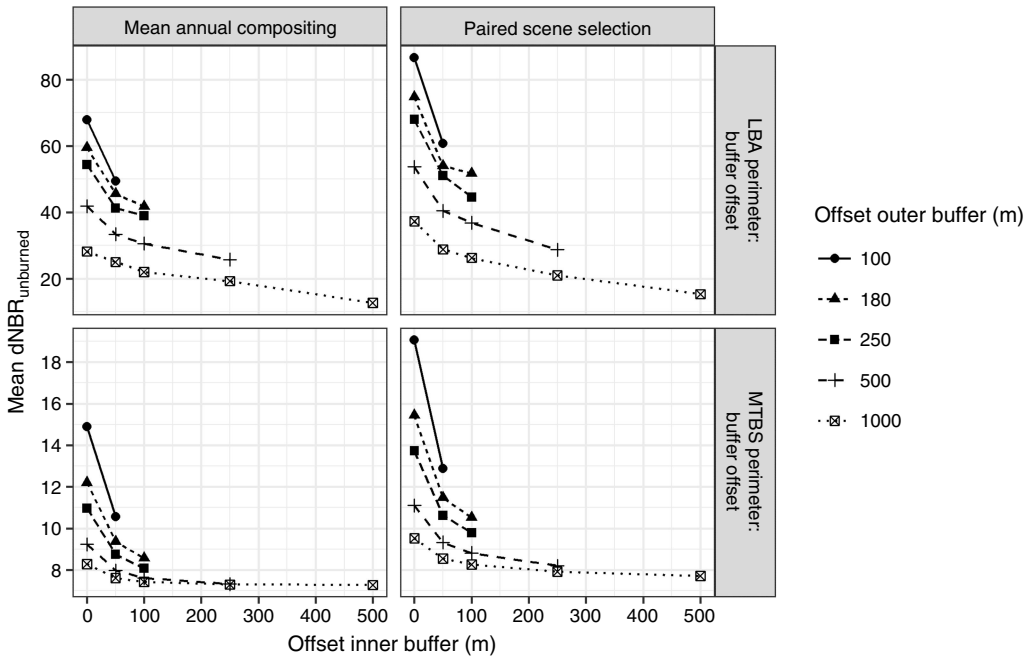

Fig. 6. Mean dNBR (differenced Normalized Burn Ratio) offset values, dNBR$_{unburned}$, across tested image selection and offset delineation methodologies for 141 fire events. We compare the influence of inner and outer ring buffer sizes derived from Monitoring Trends in Burn Severity (MTBS) and the Landsat Burned Area product (LBA) fire perimeters. The outer buffer indicates the maximum distance from the fire perimeter and the inner buffer defines the minimum distance from the fire perimeter, in between which are the pixels used to calculate the offset value.

depending on the ecosystem in consideration and methodological choices implemented.

Implications for burn severity characterization

Although offset corrections improved burn severity model performance, our analysis of dNBR$_{unburned}$ values suggests they may also introduce bias into the characterization of burn severity. In the automated offset delineation approaches, positively shifted dNBR$_{unburned}$ values suggest that offset areas may include phenologically mismatched, disturbed, or otherwise fire-affected pixels. Introduced bias may be attributed to unmapped burned pixels or unburned pixels influenced by edge effects (Braithwaite and Mallik 2012; Harper *et al.* 2015; Parkins *et al.* 2018), as shown by higher dNBR$_{unburned}$ values in offsets generated closer to fire edges, as with smaller ring buffers or pixel-based LBA perimeters. The inclusion of a positively shifted offset value in the calculation of a burn severity index will reduce the burn severity value, underestimating burn severity. Decreased severity values have been previously observed in comparisons of dNBR and automated dNBR$_{offset}$ (Parks *et al.* 2018*a*; Whitman *et al.* 2020; Morresi *et al.* 2022; Jahanianfard *et al.* 2025). Shifted dNBR severity values explain the widespread decrease in classification accuracy observed when using MTBS analyst-derived fire-specific dNBR thresholds, as offset-adjusted severity values may no longer be representative of the underlying imagery. The lack of systematic shifts following manually delineated offset correction shows that the observed bias is specific to the automated ring buffer methodologies. Analysts may provide a more consistent representation of unburned conditions by considering landscape nuance and the stratification of vegetation structure and composition in delineated offset areas. Furthermore, manual delineation may avoid inclusion of unrepresentative land-cover types (e.g. agriculture, developed) or other disturbances (e.g. insect damage, additional fire events, wildfire suppression activities) into offset areas.

Accurate definition of burn severity classes is critical for interpreting the ecological impacts of fire, informing post-fire decision-making and tracking change through time. Biased offset corrections that systematically lower severity values may misclassify low-severity burns as unburned, leading to underestimations of burned area, challenging accurate mapping of fire extent (Hawbaker *et al.* 2017; Vanderhoof *et al.* 2021). Identification of high-severity burn patches is also significant for recognizing areas of management priority (Bolton *et al.* 2015; Chambers *et al.* 2016; Harvey *et al.* 2016; Bright *et al.* 2019; Stevens-Rumann and Morgan 2019; Menick *et al.* 2024) and characterizing shifting fire regimes (Parks *et al.* 2018*b*; Singleton *et al.* 2019; Buonanduci *et al.* 2023). Bias in burn severity values is an important consideration when thresholding severity classes or making comparisons between uncorrected

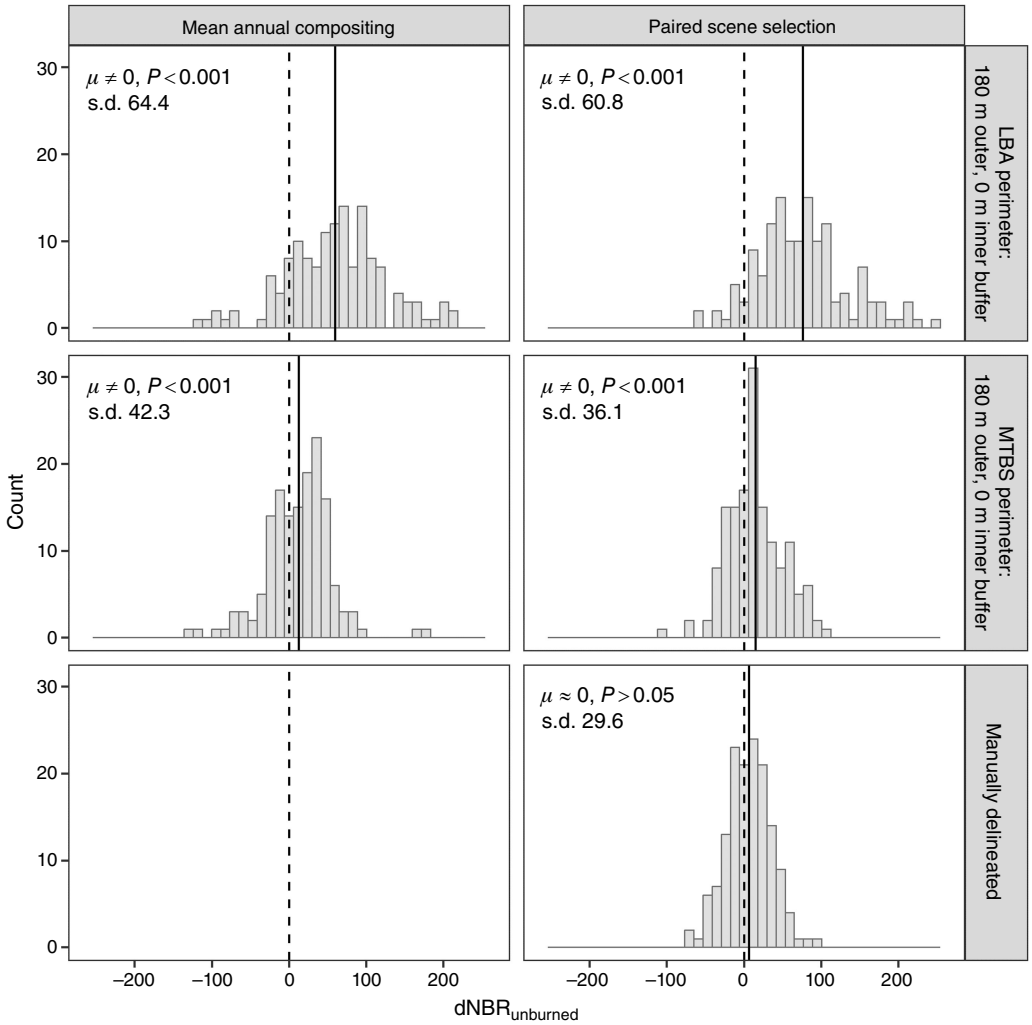

Fig. 7. Distribution of dNBR (differenced Normalized Burn Ratio) offset values, $dNBR_{unburned}$, across 141 evaluated fire events. We show the distribution of $dNBR_{unburned}$ for two common offset delineation methods, an automated approach using a fire perimeter ring buffer (180 m outer, 0 m inner) and manual delineation. The dashed line indicates a $dNBR_{unburned}$ of zero, or no difference between pre- and post-fire NBR. solid line indicates the mean $dNBR_{unburned}$ offset value. The results of a one-sample *t*-test, assessing whether the mean $dNBR_{unburned}$ (μ) differs from zero and standard deviation of $dNBR_{unburned}$ values, are overlaid.

and offset-adjusted measures of burn severity. Additional scrutiny of bias is also advisable when using an algorithmically derived burned area product or other dataset with greater fire perimeter uncertainty (Parks *et al.* 2019)

Considerations for calculating burn severity

Our findings present trade-offs when applying offset corrections in burn severity calculations. Analysts may need to consider whether the benefit from offset corrections to address phenological differences outweighs the potential to incorporate additional error. We provide considerations for applying offset corrections tailored to the specific parameters of the analysis being conducted (Fig. 8).

Severity data type: although we identified improvements from offset corrections in the continuous, modeled relationship between CBI and dNBR or RdNBR, we did not identify significant benefits from applying offset values when categorizing burn severity. Studies utilizing categorical burn severity data may not see an appreciable advantage, or even a decrease in classification accuracy, from offset correction. If offset corrections are used, analysts are encouraged to set model-specific severity thresholds.

Study scale: severity evaluations using manually delineated offsets to correct for phenological differences had equivalent modeled performance to automatically generated offsets and did not introduce directional severity shifts. However, manually delineated offsets

Table 2. Classification accuracy of field-observed severity classes by those derived from the differenced Normalized Burn Ratio (dNBR) or relativized dNBR (RdNBR).

	Model-specific regression thresholds									
	dNBR					$dNBR_{offset}$				
	Overall (%)	Unburned (%)	Low (%)	Moderate (%)	High (%)	Overall (%)	Unburned (%)	Low (%)	Moderate (%)	High (%)
Automated LBA buffer offset mean annual image composites	56.1	66.8	51.0	45.9	71.8	54.1	62.3	48.9	46.6	73.7
Automated LBA buffer offset paired scene selection	54.5	64.7	56.0	47.4	65.9	53.1	60.6	51.0	45.3	71.0
Automated MTBS buffer offset mean annual image composites	56.1	66.8	51.0	45.9	71.8	56.3	67.8	54.8	47.9	72.7
Automated MTBS buffer offset paired scene selection	54.5	64.7	56.0	47.4	65.9	55.0	64.4	58.7	46.9	67.5
Manually delineated offset paired scene selection	53.8	63.0	54.5	48.6	64.2	55.0	71.2	53.6	48.8	65.8
	Fire-specific MTBS thresholds									
	dNBR					$dNBR_{offset}$				
	Overall (%)	Unburned (%)	Low (%)	Moderate (%)	High (%)	Overall (%)	Unburned (%)	Low (%)	Moderate (%)	High (%)
Automated LBA buffer offset mean annual image composites	46.8	79.8	54.8	25.2	46.9	30.8	89.7	22.7	12.6	31.7
Automated LBA buffer offset paired scene selection	52.0	76.7	59.1	37.8	56.0	39.1	89.4	33.3	23.8	40.9
Automated MTBS buffer offset mean annual image composites	46.8	79.8	54.8	25.2	46.9	41.6	82.9	45.5	21.7	43.0
Automated MTBS buffer offset paired scene selection	52.0	76.7	59.1	37.8	56.0	49.8	79.1	56.0	34.4	53.3
Manually delineated offset paired scene selection	51.0	77.4	57.9	37.5	53.4	49.6	75.3	57.3	35.4	53.4
	Model-specific regression thresholds									
	RdNBR					$RdNBR_{offset}$				
	Overall (%)	Unburned (%)	Low (%)	Moderate (%)	High (%)	Overall (%)	Unburned (%)	Low (%)	Moderate (%)	High (%)
Automated LBA buffer offset mean annual image composites	54.9	67.5	42.9	45.7	77.9	56.3	61.0	49.9	48.8	77.5
Automated LBA buffer offset paired scene selection	55.4	71.2	51.3	48.8	69.2	56.3	59.6	52.9	47.6	70.1
Automated MTBS buffer offset mean annual image composites	54.9	67.5	42.9	45.7	77.9	56.7	70.5	49.8	47.2	77.8
Automated MTBS buffer offset paired scene selection	55.4	71.2	51.3	48.8	69.2	56.1	70.9	53.3	49.7	69.5
Manually delineated offset paired scene selection	53.4	68.8	48.6	45.9	66.5	54.1	74.3	44.6	48.0	69.5

We compare the influence of offset correction using 180 m ring buffers surrounding Landsat Burned Area (LBA) or Monitoring Trends in Burn Severity (MTBS) perimeters and manual delineation.

Table 3. Change in model RMSE following dNBR (differenced Normalized Burn Ratio) offset correction across NLCD (National Land Cover Database) landcover categories.

	dNBR				RdNBR			
	Evergreen forest	**Woody wetlands**	**Shrub–scrub**	**Grassland**	**Evergreen forest**	**Woody wetlands**	**Shrub–scrub**	**Grassland**
Automated LBA buffer offset mean annual image composites	−11.6	−32.6	−49.1	−55.5	−13.2	−77.1	−78.6	−126.5
Automated LBA buffer offset paired scene selection	−3.1	+8.4	−19.8	−6.3	−3.5	+4.3	−71.9	−129.2
Automated MTBS buffer offset mean annual image composites	−8.0	−24.0	−27.0	−41.7	−16.1	−39.5	−54.5	−72.4
Automated MTBS buffer offset paired scene selection	−1.5	+9.9	−7.3	−18.5	+3.3	+20.3	−83.7	−162.1
Manually delineated offset paired scene selection	+0.1	−0.9	−1.9	−18.3	−10.0	−8.3	−54.3	−131.4
	dNBR				**RdNBR**			
	Evergreen forest	**Woody wetlands**	**Shrub–scrub**	**Grassland**	**Evergreen forest**	**Woody wetlands**	**Shrub–scrub**	**Grassland**
Offset with more heterogeneous landcover	−2.9	−6.7	−13.3	−21.4	−6.6	−4.1	−117.3	−133.9
Offset with more homogeneous landcover	−8.9	−7.7	−36.0	−37.7	−5.4	−42.4	−46.9	−118.1
Offset with more unrepresentative landcover	−4.2	−13.1	−16.1	−20.0	−14.4	−51.9	−124.6	−159.4
Offset with more representative landcover	−7.7	−0.1	−35.1	−40.5	+6.2	+7.1	−42.2	−84.2

Negative values indicate improved predictive performance, whereas positive values suggest decreased predictive capacity by incorporating the offset value. We compare commonly utilized offset types, including manually delineated polygons and ring buffers derived from LBA (Landsat Burned Area) and MTBS (Monitoring Trends in Burn Severity) fire perimeters, as well as the influence of landcover composition within the offset area.

Table 4. Change in model RMSE following dNBR (differenced Normalized Burn Ratio) offset correction across LANDFIRE canopy cover classes.

	dNBR			RdNBR		
	Closed canopy (≥70%)	Open canopy (10–70%)	Non-forested (≤10%)	Closed canopy (≥70%)	Open canopy (10–70%)	Non-forested (≤10%)
Automated LBA buffer offset mean annual image composites	−22.8	−9.0	−70.9	−3.0	−7.3	−141.5
Automated LBA buffer offset paired scene selection	−10.2	−0.9	−23.2	+26.8	−2.2	−126.4
Automated MTBS buffer offset mean annual image composites	−9.0	−8.7	−40.6	−10.8	−7.7	−98.7
Automated MTBS buffer offset paired scene selection	+2.1	−3.0	−10.9	+1.5	+6.3	−146.4
Manually delineated offset paired scene selection	+0.5	−0.8	−6.3	−5.1	−2.9	−114.0
	dNBR			RdNBR		
	Closed canopy (≥70%)	Open canopy (10–70%)	Non-forested (≤10%)	Closed canopy (≥70%)	Open canopy (10–70%)	Non-forested (≤10%)
Offset with more heterogeneous canopy cover	−12.4	−3.5	−19.5	+16.4	−1.9	−114.9
Offset with more homogeneous canopy cover	−6.4	−7.3	−51.7	−6.4	−1.7	−132.4
Offset with more unrepresentative canopy cover	−8.4	−4.5	−18.0	4.7	−7.8	−115.6
Offset with more representative canopy cover	−10.5	−5.9	−52.9	5.2	4.5	−133.5

Negative values indicate improved predictive performance, whereas positive values suggest decreased predictive capacity by incorporating the offset value. We compare commonly utilized offset types, including manually delineated polygons and ring buffers derived from LBA (Landsat Burned Area) and MTBS (Monitoring Trends in Burn Severity) fire perimeters, as well as the influence of canopy cover composition within the offset area.

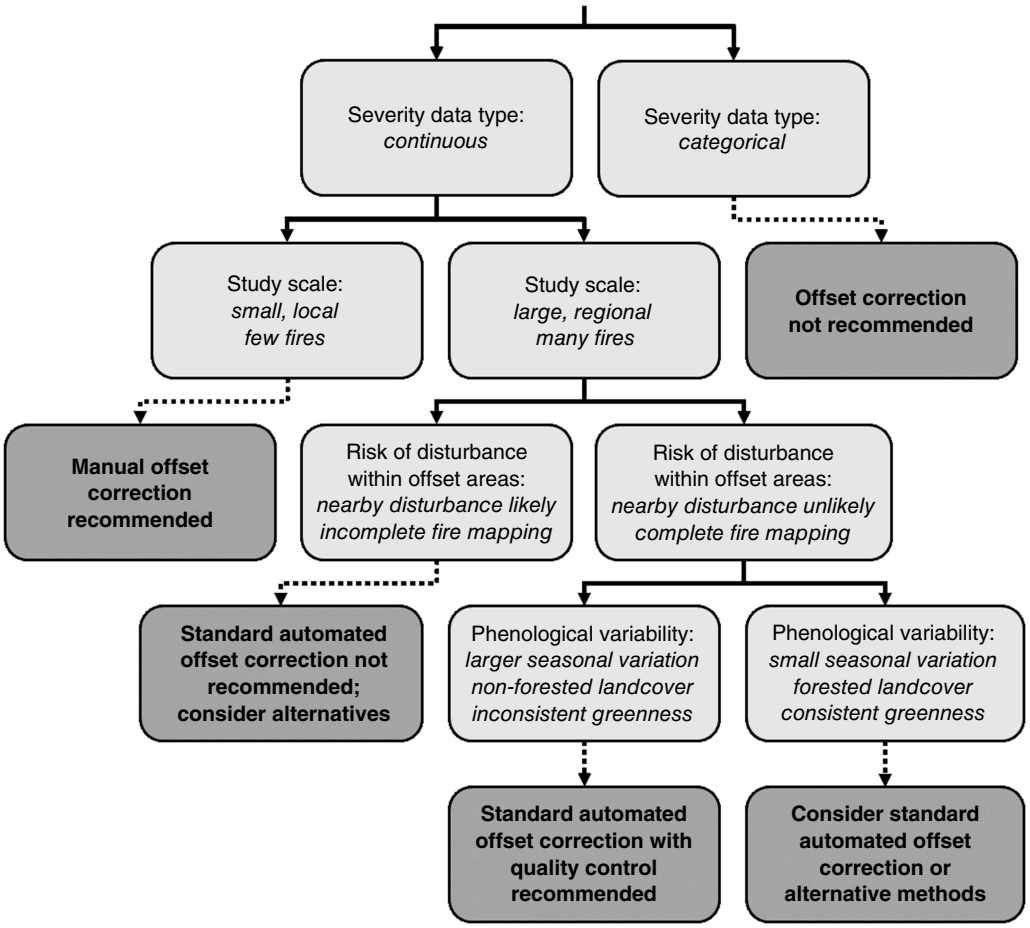

Fig. 8. Considerations for applying phenological offset corrections in the calculation of burn severity, as a decision-tree framework dependent on the study scope and characteristics of the environment to be evaluated.

are typically only feasible for smaller-scale evaluations. For larger- scale analyses, where manually generating offset values is not practical, additional considerations are needed to determine if automated correction methods are appropriate.

Potential for disturbed vegetation in automated offsets: incomplete mapping of burned area or ecosystems with frequent disturbance may affect the ability of automated buffer offsets to accurately represent vegetation conditions. The completeness and accuracy of the underlying burned area product may be considered, as mapping effort and accuracy are inconsistent across products and between ecosystem types (Eidenshink *et al.* 2007; Padilla *et al.* 2014; Vanderhoof *et al.* 2017; Boschetti *et al.* 2019; Hawbaker *et al.* 2020; Picotte *et al.* 2020; Chen *et al.* 2021). Where there is a larger risk of including disturbed pixels into an automatically generated offset area, utilizing larger ring buffer sizes, incorporating pixel masking approaches, forgoing offset correction, or employing alternative methods of phenological correction, such as time series normalization, may be considered.

Phenological variability: if large differences in pre- and post-fire imagery are anticipated, either due to imagery limitations or vegetation conditions, applying offset corrections may be more beneficial and justify the potential risk of incorporating additional error. Should the accuracy of more dynamic vegetation types (e.g. non-forested, deciduous, hydrologically sensitive) need to be prioritized, applying offset corrections or other methods to address phenological differences becomes increasingly important. Analyses utilizing image offset corrections may perform additional data checks of $dNBR_{unburned}$ offset values to support accurate, unbiased assessment of burn severity.

Limitations and future work

Although our study provides a detailed examination of the use of offset corrections in the calculation of burn severity, limitations should be considered. Our analysis was restricted the extent of the CBI dataset (Picotte *et al.* 2019), which does not fully capture or equivalently represent all fire-

prone ecosystems, vegetation conditions, or fire effects. Large-scale collections of field data are immensely valuable to inform and guide remote sensing analyses by linking remote sensing observations to physically observed fire effects. The CBI database of Picotte *et al.* (2019) has been widely used to model burn severity spectral indices (Miller *et al.* 2023), and continued expansion of similar field data campaigns are worthy of support. Although CBI was designed to provide a consistent operational measurement of burn severity and enablealignment with moderate-resolution satellite imagery (Key and Benson 2006; French *et al.* 2008; Saberi *et al.* 2022), it may not provide consistent relationships with satellite spectral indices across all environments (De Santis and Chuvieco 2009; Stambaugh *et al.* 2015; Parks *et al.* 2019).

Further exploration of methods to correct for phenological differences between pre- and post-fire imagery may be pursued to improve the consistency and representativeness of automated offset methods. Analysts may consider masking approaches to exclude extreme reflectance values, areas of known disturbance, or unrepresentative cover types (Picotte 2020; Morresi *et al.* 2022). Landcover-specific offset values could be considered to more effectively standardize measurements for different vegetation types, in particular for fire events that burn across heterogeneous landscapes. Although excluding non-representative landcover types was not previously found to benefit models of burn severity (Morresi *et al.* 2022), it is possible that generating offsets distinct to each vegetation class (e.g. grassland, evergreen forest) could be beneficial for a subset of fire events. Analysts may also consider summarizing pixel values with other statistics, such as the median or percentile values, to reduce the influence of outliers. New or alternative approaches to identify unburned pixels of similar vegetation composition may help to avoid interference estimating unchanged vegetation greenness (Lhermitte *et al.* 2010; Veraverbeke *et al.* 2010; Morresi *et al.* 2022). If representative unburned offset areas cannot be generated, other techniques of phenological standardization, such as time series normalization or reflectance correction could be considered to alternatively address phenology mismatch.

Finally, although the manual and automated approaches we utilized to characterize burn severity are reflective of the commonly employed methods within the remote sensing community, machine learning modeling offers important advances. Whereas more simplistic single spectral index regression approaches are useful for characterizing the individual influence of methodological decisions and providing interpretable results, machine learning models have been found to achieve superior predictive accuracy for burn severity classification (Meddens *et al.* 2016; Collins *et al.* 2018; Gibson *et al.* 2020) and continuous regression (Hultquist *et al.* 2014; Parks *et al.* 2019; Vanderhoof *et al.* 2025). Through decision-tree frameworks, machine learning models may incorporate multiple variables, such as additional imagery, spectral indices, vegetation structural measures, or ecosystem characteristics to improve model predictions across heterogeneous landscapes (Cutler *et al.* 2007). Our analysis may serve as a foundation for future machine learning model development by providing insight into the individual effects of key methodological choices and importance of phenological standardization. Machine learning modeling may effectively address differences in phenology through other methods of standardization, such as unburned plot locations, multiple imagery time points and landcover or climate variables. The continued development and application of advanced modeling techniques will improve future landscape-scale burn severity mapping.

Conclusion

There is a need for reliable, accurate and efficient remotely sensed techniques to evaluate burn severity at landscape scales. This study provides a novel and detailed evaluation of the impact of image offset corrections in the calculation of burn severity. Our findings demonstrate the need for intentional application of offset corrections, and the importance of weighing the potential methodological improvements at the cost of additional spectral noise, bias, or computational requirements. Consideration of the potential trade-offs identified between offset corrections mitigating extreme outlier severity values and altering the categorization of burn severity is warranted. This work is significant to operationalized burn severity products and landscape-scale studies of severity, where automated processing of satellite imagery is increasingly relied on.

References

Abatzoglou JT, Dobrowski SZ, Parks SA, Hegewisch KC (2018) TerraClimate, a high-resolution global dataset of monthly climate and climatic water balance from 1958–2015. *Scientific Data* **5**(1), 170191. doi:10.1038/sdata.2017.191

Alonso-González E, Fernández-García V (2021) MOSEV: a global burn severity database from MODIS (2000–2020). *Earth System Science Data* **13**(5), 1925–1938. doi:10.5194/essd-13-1925-2021

Bolton DK, Coops NC, Wulder MA (2015) Characterizing residual structure and forest recovery following high-severity fire in the western boreal of Canada using Landsat time-series and airborne lidar data. *Remote Sensing of Environment* **163**, 48–60. doi:10.1016/j.rse.2015.03.004

Boschetti L, Roy DP, Giglio L, Huang H, Zubkova M, Humber ML (2019) Global validation of the Collection 6 MODIS burned area product. *Remote Sensing of Environment* **235**, 111490. doi:10.1016/j.rse.2019.111490

Braithwaite NT, Mallik AU (2012) Edge effects of wildfire and riparian buffers along boreal forest streams. *Journal of Applied Ecology* **49**(1), 192–201. doi:10.1111/j.1365-2664.2011.02076.x

Bright BC, Hudak AT, Kennedy RE, Braaten JD, Henareh Khalyani A (2019) Examining post-fire vegetation recovery with Landsat time series analysis in three western North American forest types. *Fire Ecology* **15**(1), 8. doi:10.1186/s42408-018-0021-9

Buonanduci MS, Donato DC, Halofsky JS, Kennedy MC, Harvey BJ (2023) Consistent spatial scaling of high-severity wildfire can inform expected future patterns of burn severity. *Ecology Letters* **26**(10), 1687–1699. doi:10.1111/ele.14282

Cansler CA, McKenzie D (2012) How robust are burn severity indices when applied in a new region? Evaluation of alternate field-based and remote-sensing methods. *Remote Sensing* **4**(2), 456–483. doi:10.3390/rs4020456

Chambers ME, Fornwalt PJ, Malone SL, Battaglia MA (2016) Patterns of conifer regeneration following high severity wildfire in ponderosa pinedominated forests of the Colorado Front Range. *Forest Ecology and Management* **378**, 57–67. doi:10.1016/j.foreco.2016.07.001

Chandler JR, Parks SA, Hoecker TJ, Cansler CA, Dobrowski SZ (2024) Wildfires Are Burning Less Frequently and More Severely in the Western US: An Integrative Approach to Calculating Fire-Regime Departures [Preprint]. doi:10.21203/rs.3.rs-5270701/v1

Chen D, Shevade V, Baer A, Loboda TV (2021) Missing burns in the High Northern Latitudes: the case for regionally focused burned area products. *Remote Sensing* **13**(20), 4145. doi:10.3390/rs13204145

Chuvieco E, Mouillot F, Van Der Werf GR, San Miguel J, Tanase M, Koutsias N, García M, Yebra M, Padilla M, Gitas I, Heil A, Hawbaker TJ, Giglio L (2019) Historical background and current developments for mapping burned area from satellite Earth observation. *Remote Sensing of Environment* **225**, 45–64. doi:10.1016/j.rse.2019.02.013

Collins L, Griffioen P, Newell G, Mellor A (2018) The utility of Random Forests for wildfire severity mapping. *Remote Sensing of Environment* **216**, 374–384. doi:10.1016/j.rse.2018.07.005

Coop JD, Parks SA, Stevens-Rumann CS, Crausbay SD, Higuera PE, Hurteau MD, Tepley A, Whitman E, Assal T, Collins BM, Davis KT, Dobrowski S, Falk DA, Fornwalt PJ, Fulé PZ, Harvey BJ, Kane VR, Littlefield CE, Margolis EQ, North M, Parisien MA, Prichard S, Rodman KC (2020) Wildfire-Driven Forest conversion in western North American landscapes. *BioScience* **70**(8), 659–673. doi:10.1093/biosci/biaa061

Cummins K, Noble J, Varner JM, Robertson KM, Hiers JK, Nowell HK, Simonson E (2023) The Southeastern US Prescribed Fire Permit Database: Hot Spots and Hot Moments in Prescribed Fire across the Southeastern USA. *Fire* **6**(10), 372. doi:10.3390/fire6100372

Cutler DR, Edwards TC Jr, Beard KH, Cutler A, Hess KT, Gibson J, Lawler JJ (2007) Random Forests for classification in ecology. *Ecology* **88**(11), 2783–2792. doi:10.1890/07-0539.1

Dennison PE, Brewer SC, Arnold JD, Moritz MA (2014) Large wildfire trends in the western United States, 1984–2011. *Geophysical Research Letters* **41**(8), 2928–2933. doi:10.1002/2014GL059576

De Santis A, Chuvieco E (2009) GeoCBI: a modified version of the Composite Burn Index for the initial assessment of the short-term burn severity from remotely sensed data. *Remote Sensing of Environment* **113**(3), 554–562. doi:10.1016/j.rse.2008.10.011

Dunn CJ, O'Connor CD, Reilly MJ, Calkin DE, Thompson MP (2019) Spatial and temporal assessment of responder exposure to snag hazards in post-fire environments. *Forest Ecology and Management* **441**, 202–214. doi:10.1016/j.foreco.2019.03.035

Eidenshink J, Schwind B, Brewer K, Zhu Z-L, Quayle B, Howard S (2007) A project for monitoring trends in burn severity. *Fire Ecology Special Issue* **3**(1), 3–21. doi:10.4996/fireecology.0301003

Elvidge CD (1990) Visible and near-infrared reflectance characteristics of dry plant materials. *International Journal of Remote Sensing* **11**(10), 1775–1795. doi:10.1080/01431169008955129

Farasin A, Colomba L, Garza P (2020) Double-Step U-Net: A Deep Learning-Based Approach for the estimation of wildfire damage severity through Sentinel-2 Satellite data. *Applied Sciences* **10**(12), 4332. doi:10.3390/app10124332

Foga S, Scaramuzza PL, Guo S, Zhu Z, Dilley RD, Beckmann T, Schmidt GL, Dwyer JL, Joseph Hughes M, Laue B (2017) Cloud detection algorithm comparison and validation for operational Landsat data products. *Remote Sensing of Environment* **194**, 379–390. doi:10.1016/j.rse.2017.03.026

Fontaine JB, Kennedy PL (2012) Meta-analysis of avian and small-mammal response to fire severity and fire surrogate treatments in U.S. fire-prone forests. *Ecological Applications* **22**(5), 1547–61. doi:10.1890/12-0009.1

French NHF, Kasischke ES, Hall RJ, Murphy KA, Verbyla DL, Hoy EE, Allen JL (2008) Using Landsat data to assess fire and burn severity in the North American boreal forest region: an overview and summary of results. *International Journal of Wildland Fire* **17**(4), 443–462. doi:10.1071/WF08007

García MJL, Caselles V (1991) Mapping burns and natural reforestation using Thematic Mapper data. *Geocarto International* **6**(1), 31–37. doi:10.1080/10106049109354290

Gibson R, Danaher T, Hehir W, Collins L (2020) A remote sensing approach to mapping fire severity in south-eastern Australia using Sentinel 2 and random forest. *Remote Sensing of Environment* **240**, 111702. doi:10.1016/j.rse.2020.111702

Giglio L, Boschetti L, Roy DP, Humber ML, Justice CO (2018) The Collection 6 MODIS burned area mapping algorithm and product. *Remote Sensing of Environment* **217**, 72–85. doi:10.1016/j.rse.2018.08.005

Girona-García A, Vieira DCS, Silva J, Fernández C, Robichaud PR, Keizer JJ (2021) Effectiveness of post-fire soil erosion mitigation treatments: a systematic review and meta-analysis. *Earth-Science Reviews* **217**, 103611. doi:10.1016/j.earscirev.2021.103611

Hall J, Sandor ME, Harvey BJ, Parks SA, Trugman AT, Williams AP, Hansen WD (2024) Forest carbon storage in the western United States: distribution, drivers, and trends. *Earth's Future* **12**(7), e2023EF004399. doi:10.1029/2023EF004399

Harper KA, Macdonald SE, Mayerhofer MS, Biswas SR, Esseen P, Hylander K, Stewart KJ, Mallik AU, Drapeau P, Jonsson B, Lesieur D, Kouki J, Bergeron Y (2015) Edge influence on vegetation at natural and anthropogenic edges of boreal forests in Canada and Fennoscandia. *Journal of Ecology* **103**(3), 550–562. doi:10.1111/1365-2745.12398

Harvey BJ, Donato DC, Turner MG (2016) High and dry: post-fire tree seedling establishment in subalpine forests decreases with post-fire drought and large stand-replacing burn patches. *Global Ecology and Biogeography* **25**(6), 655–669. doi:10.1111/geb.12443

Hawbaker TJ, Vanderhoof MK, Beal Y-J, Takacs JD, Schmidt GL, Falgout JT, Williams B, Fairaux NM, Caldwell MK, Picotte JJ, Howard SM, Stitt S, Dwyer JL (2017) Mapping burned areas using dense time-series of Landsat data. *Remote Sensing of Environment* **198**, 504–522. doi:10.1016/j.rse.2017.06.027

Hawbaker TJ, Vanderhoof MK, Schmidt GL, Beal Y-J, Picotte JJ, Takacs JD, Falgout JT, Dwyer JL (2020) The Landsat Burned Area algorithm and products for the conterminous United States. *Remote Sensing of Environment* **244**, 111801. doi:10.1016/j.rse.2020.111801

Hawbaker TJ, Henne PD, Vanderhoof MK, Carlson AR, Mockrin MH, Radeloff VC (2023) Changes in wildfire occurrence and risk to homes from 1990 through 2019 in the Southern Rocky Mountains, USA. *Ecosphere* **14**(2), e4403. doi:10.1002/ecs2.4403

He K, Shen X, Anagnostou EN (2024) A global forest burn severity dataset from Landsat imagery (2003–2016). *Earth System Science Data* **16**(6), 3061–3081. doi:10.5194/essd-16-3061-2024

Holden ZA, Warren D, Davis K, Jungck E, Maneta M, Dobrowski S, Archer V (2022) REGEN MAPPER: A Web-Based Tool for Predicting Postfire Conifer Regeneration and Prioritizing Reforestation Efforts in the Western United States. In 'Foundational concepts in silviculture with emphasis on reforestation and early stand improvement - 2022 National Silviculture Workshop.' Proc. RMRS-P-80'. (Eds TB Jain, TM Schuler) 2 p. (USDA Forest Service, Rocky Mountain Research Station: Fort Collins, CO)

Holsinger LM, Parks SA, Saperstein LB, Loehman RA, Whitman E, Barnes J, Parisien M (2022) Improved fire severity mapping in the North American boreal forest using a hybrid composite method. *Remote Sensing in Ecology and Conservation* **8**(2), 222–235. doi:10.1002/rse2.238

Howe AA, Parks SA, Harvey BJ, Saberi SJ, Lutz JA, Yocom LL (2022) Comparing Sentinel-2 and Landsat 8 for Burn Severity Mapping in Western North America. *Remote Sensing* **14**(20), 5249. doi:10.3390/rs14205249

Hultquist C, Chen G, Zhao K (2014) A comparison of Gaussian process regression, random forests and support vector regression for burn severity assessment in diseased forests. *Remote Sensing Letters* **5**(8), 723–732. doi:10.1080/2150704X.2014.963733

Jahanianfard D, Parente J, Gonzalez-Pelayo O, Benali A (2025) Multidecadal satellite-derived Portuguese Burn Severity Atlas (1984–2022). *Earth System Science Data* **17**, 4957–4984. doi:10.5194/essd-17-4957-2025

Keeley JE (2009) Fire intensity, fire severity and burn severity: a brief review and suggested usage. *International Journal of Wildland Fire* **18**(1), 116–126. doi:10.1071/WF07049

Key C (2005) Remote sensing sensitivity to fire severity and fire recovery. In '5th international workshop on remote sensing and GIS applications to forest fire management: Fire effects assessment,' 16 June 2005. (Eds J De la Riva, F Perez-Cabello, E Chuvieco) pp. 29–39. (Universidad de Zaragoza: Spain) https://pubs.usgs.gov/publication/70160111

Key CH, Benson NC (2006) Landscape Assessment (LA) Sampling and Analysis Methods. In 'FIREMON: Fire effects monitoring and inventory system.' Gen. Tech. Report RMRS-GTR-164-CD. (Eds DC Lutes, RE Keane, JF Caratti, CH Key, NC Benson, S Sutherland, LJ Gangi) pp. LA1–LA55. (USDA Forest Service, Rocky Mountain Research Station: Fort Collins, CO)

Kobziar L, Godwin D, Taylor L, Watts A (2015) Perspectives on trends, effectiveness, and impediments to prescribed burning in the southern US. *Forests* **6**(12), 561–580. doi:10.3390/f6030561

Kolden CA, Weisberg PJ (2007) Assessing accuracy of manually-mapped wildfire perimeters in topographically dissected areas. *Fire Ecology* **3**(1), 22–31. doi:10.4996/fireecology.0301022

Lentile LB, Morgan P, Hudak AT, Bobbitt MJ, Lewis SA, Smith AMS, Robichaud PR, Morgan P, Hudak AT, Bobbitt MJ, Lewis SA, Smith AMS (2007) Post-fire burn severity and vegetation response following eight large wildfires across the western United States. *Fire Ecology* **3**, 91–108. doi:10.4996/fireecology.0301091

Lewis JS, LeSueur L, Oakleaf J, Rubin ES (2022) Mixed-severity wildfire shapes habitat use of large herbivores and carnivores. *Forest Ecology and Management* **506**, 119933. doi:10.1016/j.foreco.2021.119933

Lhermitte S, Verbesselt J, Verstraeten WW, Coppin P (2010) A pixel based regeneration index using time series similarity and spatial context. *Photogrammetric Engineering & Remote Sensing* **76**(6), 673–682. doi:10.14358/PERS.76.6.673

Lobell DB, Asner GP (2002) Moisture effects on soil reflectance. *Soil Science Society of America Journal* **66**(3), 722–727. doi:10.2136/sssaj2002.7220

Lydersen JM, Collins BM, Miller JD, Fry DL, Stephens SL (2016) Relating fire-caused change in forest structure to remotely sensed estimates of fire severity. *Fire Ecology* **12**(3), 99–116. doi:10.4996/fireecology.1203099

McGuire LA, Ebel BA, Rengers FK, Vieira DCS, Nyman P (2024) Fire effects on geomorphic processes. *Nature Reviews Earth & Environment* **5**(7), 486–503. doi:10.1038/s43017-024-00557-7

Meddens AJH, Kolden CA, Lutz JA (2016) Detecting unburned areas within wildfire perimeters using Landsat and ancillary data across the northwestern United States. *Remote Sensing of Environment* **186**, 275–285. doi:10.1016/j.rse.2016.08.023

Meigs GW, Donato DC, Campbell JL, Martin JG, Law BE (2009) Forest fire impacts on carbon uptake, storage, and emission: the role of burn severity in the Eastern Cascades, Oregon. *Ecosystems* **12**(8), 1246–1267. doi:10.1007/s10021-009-9285-x

Melaas EK, Friedl MA, Zhu Z (2013) Detecting interannual variation in deciduous broadleaf forest phenology using Landsat TM/ETM+ data. *Remote Sensing of Environment* **132**, 176–185. doi:10.1016/j.rse.2013.01.011

Menick C, Tinkham W, Hoffman C, Vanderhoof M, Vogeler J (2024) Snow-cover remote sensing of conifer tree recovery in high-severity burn patches. *Remote Sensing of Environment* **305**, 114114. doi:10.1016/j.rse.2024.114114

Menick C, Vanderhoof M, Picotte J, Reiner A, Chastain (2025) Generated Burn Severity Offset Correction Values for a Composite Burn Index Field Plot Dataset. (US Geological Survey data release). doi:10.5066/P14VCK4T

Miller CW, Harvey BJ, Kane VR, Moskal LM, Alvarado E (2023) Different approaches make comparing studies of burn severity challenging: a review of methods used to link remotely sensed data with the Composite Burn Index. *International Journal of Wildland Fire* **32**(4), 449–475. doi:10.1071/WF22050

Miller JD, Thode AE (2007) Quantifying burn severity in a heterogeneous landscape with a relative version of the delta Normalized Burn Ratio (dNBR). *Remote Sensing of Environment* **109**(1), 66–80. doi:10.1016/j.rse.2006.12.006

Miller JD, Knapp EE, Key CH, Skinner CN, Isbell CJ, Creasy RM, Sherlock JW (2009) Calibration and validation of the relative differenced Normalized Burn Ratio (RdNBR) to three measures of fire severity in the Sierra Nevada and Klamath Mountains, California, USA. *Remote Sensing of Environment* **113**(3), 645–656. doi:10.1016/j.rse.2008.11.009

Moody JA, Martin DA, Haire SL, Kinner DA (2008) Linking runoff response to burn severity after a wildfire. *Hydrological Processes* **22**(13), 2063–2074. doi:10.1002/hyp.6806

Morresi D, Marzano R, Lingua E, Motta R, Garbarino M (2022) Mapping burn severity in the western Italian Alps through phenologically coherent reflectance composites derived from Sentinel-2 imagery. *Remote Sensing of Environment* **269**, 112800. doi:10.1016/j.rse.2021.112800

Padilla M, Stehman SV, Chuvieco E (2014) Validation of the 2008 MODIS-MCD45 global burned area product using stratified random sampling. *Remote Sensing of Environment* **144**, 187–196. doi:10.1016/j.rse.2014.01.008

Parkins K, York A, Di Stefano J (2018) Edge effects in fire-prone landscapes: ecological importance and implications for fauna. *Ecology and Evolution* **8**(11), 5937–5948. doi:10.1002/ece3.4076

Parks SA, Abatzoglou JT (2020) Warmer and drier fire seasons contribute to increases in area burned at high severity in Western US Forests from 1985 to 2017. *Geophysical Research Letters* **47**(22), e2020GL089858. doi:10.1029/2020GL089858

Parks SA, Dillon GK, Miller C (2014) A new metric for quantifying burn severity: the Relativized Burn Ratio. *Remote Sensing* **6**(3), 1827–1844. doi:10.3390/rs6031827

Parks SA, Holsinger LM, Voss MA, Loehman RA, Robinson NP (2018*a*) Mean composite fire severity metrics computed with Google Earth Engine offer improved accuracy and expanded mapping potential. *Remote Sensing* **10**(6), 879. doi:10.3390/rs10060879

Parks SA, Holsinger LM, Panunto MH, Jolly WM, Dobrowski SZ, Dillon GK (2018*b*) High-severity fire: evaluating its key drivers and mapping its probability across western US forests. *Environmental Research Letters* **13**(4), 44037. doi:10.1088/1748-9326/aab791

Parks SA, Holsinger LM, Koontz MJ, Collins L, Whitman E, Parisien M-A, Loehman RA, Barnes JL, Bourdon J-F, Boucher J, Boucher Y, Caprio AC, Collingwood A, Hall RJ, Park J, Saperstein LB, Smetanka C, Smith RJ, Soverel N (2019) Giving ecological meaning to satellite-derived fire severity metrics across North American forests. *Remote Sensing* **11**(14), 1735. doi:10.3390/rs11141735

Partheepan S, Sanati F, Hassan J (2025) Modelling bushfire severity and predicting future trends in Australia using remote sensing and machine learning. *Environmental Modelling & Software* **188**, 106377. doi:10.1016/j.envsoft.2025.106377

Picotte JJ (2020) Development of a New Open-Source Tool to Map Burned Area and Burn Severity. In 'Proceedings of the Fire Continuum Conference'. (Eds S Hood, S Drury, T Steelman, R Steffens) pp. 182–194. (U.S. Department of Agriculture, Forest Service, Rocky Mountain Research Station: Fort Collins, CO).

Picotte JJ, Robertson KM (2011) Validation of remote sensing of burn severity in south-eastern US ecosystems. *International Journal of Wildland Fire* **20**(3), 453–464. doi:10.1071/WF10013

Picotte JJ, Peterson B, Meier G, Howard SM (2016) 1984–2010 trends in fire burn severity and area for the conterminous US. *International Journal of Wildland Fire* **25**(4), 413–420. doi:10.1071/WF15039

Picotte JJ, Arkle R, Bastian H, Benson N, Cansler A, Caprio T, Dillon G, Key C, Klein RN, Kopper K, Meddens AJH, Ohlen D, Parks SA, Peterson DW, Pilliod D, Pritchard S, Robertson K, Sparks A, Thode A (2019) Composite Burn Index (CBI) Data for the Conterminous US, Collected Between 1996 and 2018. (US Geological Survey). doi:10.5066/P91BH1BZ

Picotte JJ, Bhattarai K, Howard D, Lecker J, Epting J, Quayle B, Benson N, Nelson K (2020) Changes to the Monitoring Trends in Burn Severity program mapping production procedures and data products. *Fire Ecology* **16**(1), 16. doi:10.1186/s42408-020-00076-y

Radeloff VC, Helmers DP, Kramer HA, Mockrin MH, Alexandre PM, Bar-Massada A, Butsic V, Hawbaker TJ, Martinuzzi S, Syphard AD, Stewart SI (2018) Rapid growth of the US wildland–urban interface raises wildfire risk. *Proceedings of the National Academy of Sciences* **115**(13), 3314–3319. doi:10.1073/pnas.1718850115

Reed BC, Brown JF, VanderZee D, Loveland TR, Merchant JW, Ohlen DO (1994) Measuring phenological variability from satellite imagery. *Journal of Vegetation Science* **5**(5), 703–714. doi:10.2307/3235884

Reiner AL, Baker C, Wahlberg M, Rau BM, Birch JD (2022) Region-specific remote-sensing models for predicting burn severity, basal area change, and canopy cover change following fire in the southwestern United States. *Fire* **5**(5), 137. doi:10.3390/fire5050137

Ruefenacht B, Finco MV, Nelson MD, Czaplewski R, Helmer EH, Blackard JA, Holden GR, Lister AJ, Salajanu D, Weyermann D, Winterberger K (2008) Conterminous U.S. and Alaska forest type mapping using forest inventory and analysis data. *Photogrammetric Engineering & Remote Sensing* **74**(11), 1379–1388. doi:10.14358/PERS.74.11.1379

Rust AJ, Saxe S, McCray J, Rhoades CC, Hogue TS (2019) Evaluating the factors responsible for post-fire water quality response in forests of the western USA. *International Journal of Wildland Fire* **28**(10), 769–784. doi:10.1071/WF18191

Saberi SJ, Harvey BJ (2023) What is the color when black is burned? Quantifying (re)burn severity using field and satellite remote sensing indices. *Fire Ecology* **19**(1), 24. doi:10.1186/s42408-023-00178-3

Saberi SJ, Agne MC, Harvey BJ (2022) Do you CBI what I see? The relationship between the Composite Burn Index and quantitative field measures of burn severity varies across gradients of forest structure. *International Journal of Wildland Fire* **31**(2), 112–123. doi:10.1071/WF21062

Shakesby RA, Doerr SH (2006) Wildfire as a hydrological and geomorphological agent. *Earth-Science Reviews* **74**(3–4), 269–307. doi:10.1016/j.earscirev.2005.10.006

Singleton MP, Thode AE, Sánchez Meador AJ, Iniguez JM (2019) Increasing trends in high-severity fire in the southwestern USA from 1984 to 2015. *Forest Ecology and Management* **433**, 709–719. doi:10.1016/j.foreco.2018.11.039

Staley DM, Tillery AC, Kean JW, McGuire LA, Pauling HE, Rengers FK, Smith JB (2018) Estimating post-fire debris-flow hazards prior to wildfire using a statistical analysis of historical distributions of fire severity from remote sensing data. *International Journal of Wildland Fire* **27**(9), 595–608. doi:10.1071/WF17122

Stambaugh M, Hammer L, Godfrey R (2015) Performance of burn-severity metrics and classification in Oak woodlands and grasslands. *Remote Sensing* **7**(8), 10501–10522. doi:10.3390/rs70810501

Steel ZL, Fogg AM, Burnett R, Roberts LJ, Safford HD (2022) When bigger isn't better—Implications of large high-severity wildfire patches for avian diversity and community composition. *Diversity and Distributions* **28**(3), 439–453. doi:10.1111/ddi.13281

Stevens-Rumann CS, Morgan P (2019) Tree regeneration following wildfires in the western US: a review. *Fire Ecology* **15**(1), 1–7. doi:10.1186/s42408-019-0032-1

Ulsig L, Nichol C, Huemmrich K, Landis D, Middleton E, Lyapustin A, Mammarella I, Levula J, Porcar-Castell A (2017) Detecting inter-annual variations in the phenology of evergreen conifers using long-term MODIS vegetation index time series. *Remote Sensing* **9**(1), 49. doi:10.3390/rs9010049

US Geological Survey (2025) Annual National Land Cover Database (NLCD) Collection 1 Products (ver. 1.1, June 2025). (US Geological Survey). doi:10.5066/P94UXNTS

Vanderhoof MK, Fairaux N, Beal Y-JG, Hawbaker TJ (2017) Validation of the USGS Landsat Burned Area Essential Climate Variable (BAECV) across the conterminous United States. *Remote Sensing of Environment* **198**, 393–406. doi:10.1016/j.rse.2017.06.025

Vanderhoof MK, Hawbaker TJ, Teske C, Ku A, Noble J, Picotte J (2021) Mapping wetland burned area from Sentinel-2 across the southeastern United States and its contributions relative to Landsat-8 (2016–2019). *Fire* **4**(3), 52. doi:10.3390/fire4030052

Vanderhoof MK, Menick CE, Picotte JJ, Robertson KM, Nowell HK, Matechik C, Hawbaker TJ (2025) Modelling and mapping burn severity of prescribed and wildfires across the southeastern United States (2000–2022). *International Journal of Wildland Fire* **34**(1), WF24137. doi:10.1071/WF24137

Veraverbeke S, Lhermitte S, Verstraeten WW, Goossens R (2010) The temporal dimension of differenced Normalized Burn Ratio (dNBR) fire/burn severity studies: the case of the large 2007 Peloponnese wildfires in Greece. *Remote Sensing of Environment* **114**(11), 2548–2563. doi:10.1016/j.rse.2010.05.029

Vieira DCS, Fernández C, Vega JA, Keizer JJ (2015) Does soil burn severity affect the post-fire runoff and interrill erosion response? A review based on meta-analysis of field rainfall simulation data. *Journal of Hydrology* **523**, 452–464. doi:10.1016/j.jhydrol.2015.01.071

White JD, Ryan KC, Key CC, Running SW (1996) Remote sensing of forest fire severity and vegetation recovery. *International Journal of Wildland Fire* **6**(3), 125–136. doi:10.1071/WF9960125

Whitman E, Parisien M-A, Holsinger LM, Park J, Parks SA (2020) A method for creating a burn severity atlas: an example from Alberta, Canada. *International Journal of Wildland Fire* **29**(11), 995–1008. doi:10.1071/WF19177

Wigtil G, Hammer RB, Kline JD, Mockrin MH, Stewart SI, Roper D, Radeloff VC (2016) Places where wildfire potential and social vulnerability coincide in the coterminous United States. *International Journal of Wildland Fire* **25**(8), 896–908. doi:10.1071/WF15109

Wong CYS, Gamon JA (2015) The photochemical reflectance index provides an optical indicator of spring photosynthetic activation in evergreen conifers. *New Phytologist* **206**(1), 196–208. doi:10.1111/nph.13251

Yang J, Tian H, Tao B, Ren W, Pan S, Liu Y, Wang Y (2015) A growing importance of large fires in conterminous United States during 1984–2012. *Journal of Geophysical Research: Biogeosciences* **120**(12), 2625–2640. doi:10.1002/2015JG002965

Data availability. The novel data produced by this project are available for download (Menick *et al.* 2025). The CBI plot data are available from Picotte *et al.* (2019).

Conflicts of interest. The authors declare they have no conflicts of interest.

Declaration of funding. We acknowledge funding for this research from the US Geological Survey's Core Science Systems Mission Area, National Land Imaging Program, Land Change Science Program as well as the US Department of Agriculture, Natural Resources Conservation Service ('SE FireMap, Phase 2 – Enhanced burned area products and decision support tools' project, Agreement no. NRC23IRA0011266).

Acknowledgements. We appreciate feedback and comments on earlier versions from Christopher Barber, Nate Benson, Brad Quayle, Craig Baker, Mark Nigrelli, Michael Bogle, Benjamin Olimpio and the journal reviewers. Any use of trade, firm, or product names is for descriptive purposes only and does not imply endorsement by the US Government.

Author affiliations

[A]US Geological Survey, Geosciences and Environmental Change Science Center, Denver Federal Center, MS980, Denver, CO 80225, USA.

[B]US Geological Survey, Earth Resources Observation and Science (EROS) Center, Sioux Falls, SD 57198, USA.

[C]Geospatial Technology and Applications Center, USDA Forest Service, Asheville, NC, USA.

[D]RedCastle Resources, Inc. Contractor to: USDA Forest Service Geospatial Technology and Applications Center (GTAC), Salt Lake City, UT 84119, USA.